

A New Family of Regularized Kernels for the Harmonic Oscillator

Benjamin W. Ong · Andrew J. Christlieb ·
Bryan D. Quaife

Received: September 7, 2018

Abstract In this paper, a new two-parameter family of regularized kernels is introduced, suitable for applying high-order time stepping to N-body systems. These high-order kernels are derived by truncating a Taylor expansion of the non-regularized kernel about $(r^2 + \epsilon^2)$, generating a sequence of increasingly more accurate kernels. This paper proves the validity of this two-parameter family of regularized kernels, constructs error estimates, and illustrates the benefits of using high-order kernels through numerical experiments.

Keywords Kernel regularization, singular integrals, N-body systems, high-order time stepping

Mathematics Subject Classification (2000) 65B99, 65P10, 70-08, 70F10, 70H05

1 Introduction

1.1 Problem statement

This paper is concerned with solutions to the system

$$\ddot{\mathbf{x}}_j = - \sum_{k \neq j} w_{jk} \nabla G(\mathbf{x}_j - \mathbf{x}_k), \quad (1)$$

Benjamin W. Ong
Mathematical Sciences, Michigan Technological University, Houghton, MI, 49931
ongbw@mtu.edu

Andrew J. Christlieb
Dept. of Mathematics, Michigan State University, East Lansing, MI, 48824
andrewch@msu.edu

Bryan D. Quaife
Department of Scientific Computing, Florida State University, Tallahassee, FL, 32306
bquaife@fsu.edu

where w_{jk} are constants, and G is the fundamental solution to Laplace's equation. Specifically,

$$G(r) = \begin{cases} -\frac{r}{2} & \text{in } \mathbb{R}^1, \\ -\frac{\ln r}{2\pi} & \text{in } \mathbb{R}^2, \\ \frac{1}{4\pi r} & \text{in } \mathbb{R}^3, \end{cases}$$

where $r = \|\mathbf{x}\|_2$. Henceforth, $\|\cdot\|_2$ is denoted as $\|\cdot\|$. System (1), modulo a change in sign, arises in many dynamical systems such as the dynamics of charged particles [13], vortex dynamics [16, 25], and planetary motions [1]. The weights w_{jk} can be interpreted as the interaction between point masses at x_j and x_k , or viewed as quadrature weights that approximate interactions due to a distribution of masses. By taking the first integral of system (1), the Hamiltonian is obtained,

$$H(\mathbf{x}, \dot{\mathbf{x}}) = \frac{1}{2} \sum_j \|\dot{\mathbf{x}}_j\|^2 + \sum_j \sum_{k \neq j} w_{jk} G(\mathbf{x}_j - \mathbf{x}_k),$$

which is a conserved quantity.

In numerical simulations, controlling the error in the Hamiltonian is of the utmost importance. Special classes of integrators, such as symplectic integrators [9, 21] or energy-conserving integrators [8], have been designed to help preserve either the symplectic structure of the equations (thereby adding stability and controlling the Hamiltonian error in some fashion as the simulation progresses), or explicitly conserving the Hamiltonian. If a fourth-order symplectic integrator [9] with a modest time step is used to solve a 25-body problem in \mathbb{R}^2 with $w_{jk} = \pm 1$, the error in the Hamiltonian rises quickly; in fact, each rise or dip corresponds to when particles cross each other. This is illustrated in the left plot of Figure 1. A convergence study shows poor convergence to the true Hamiltonian for larger Δt before fourth-order convergence is observed for sufficiently small Δt . The results of the convergence study is illustrated in the right plot of Figure 1.

A common way to overcome the reduced order of accuracy is to solve a regularized system instead of the original system,

$$\ddot{\mathbf{x}}_j = - \sum_{k \neq j} w_{jk} \nabla G^\epsilon(\mathbf{x}_j - \mathbf{x}_k), \quad (2)$$

which has the modified Hamiltonian

$$H^\epsilon(\mathbf{x}, \dot{\mathbf{x}}) = \frac{1}{2} \sum_j \|\dot{\mathbf{x}}_j\|^2 + \sum_j \sum_{k \neq j} w_{jk} G^\epsilon(\mathbf{x}_j - \mathbf{x}_k).$$

The following algebraic regularization have been used in plasma and vortex simulations [5, 18],

$$G^\epsilon(r) = \begin{cases} -\frac{1}{2} \sqrt{r^2 + \epsilon^2} & \text{in } \mathbb{R}^1, \\ -\frac{\ln \sqrt{r^2 + \epsilon^2}}{2\pi} & \text{in } \mathbb{R}^2, \\ \frac{1}{4\pi \sqrt{r^2 + \epsilon^2}} & \text{in } \mathbb{R}^3. \end{cases} \quad (3)$$

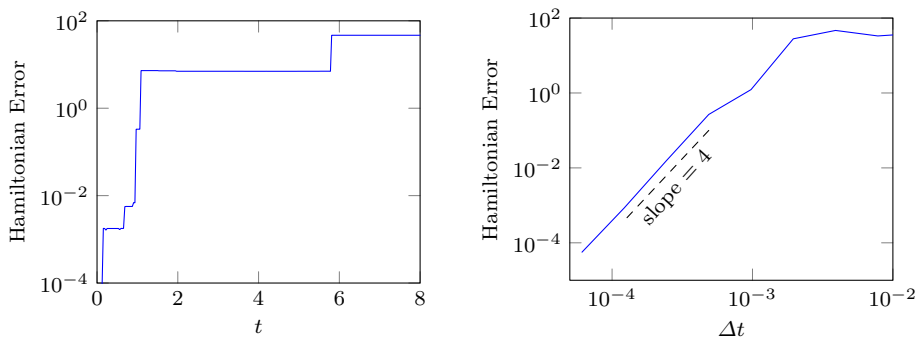


Fig. 1: *Left:* The Hamiltonian as a function of time when equation (1) is integrated with a fourth-order symplectic integrator with $\Delta t = 3.91 \times 10^{-3}$. *Right:* The error of the Hamiltonian at the time horizon $T = 8$ for various time step sizes. Fourth-order convergence is eventually attained for small time steps. The dashed black line indicates fourth-order convergence.

We shall refer to this algebraic regularization as the one-parameter family of regularized kernels. In Figure 2, the same fourth-order symplectic integrator is used to solve system (2) for the same 25-body system described earlier. Two different values of ϵ are used to specify the regularized kernel. The regularized system achieves fourth-order accuracy for large time step sizes. However for small time steps, the error stagnates; the value at which the error stagnates corresponds to the difference between the unregularized and regularized Hamiltonians, $|H(0) - H^\epsilon(0)|$. We shall refer to this difference as modelling error. This modelling error is observed in the left plot of Figure 2 at $t = 0$.

The modelling error can be reduced by decreasing ϵ . However, this results in steeper derivatives of $G^\epsilon(r)$, creating larger jumps in the Hamiltonian error (for large time steps) as two particles pass one another. The left plot of Figure 2 demonstrates this behavior. The net effect, as can be seen in the right plot of Figure 2, is that smaller values of ϵ require smaller time step sizes before the smaller modelling error is realized. This paper constructs a two-parameter family of regularized kernels that allows an integrator to achieve small modelling error with large time steps.

1.2 Related work

One approach for forming a regularization is to solve $\mathcal{L}G^\epsilon = \delta_\epsilon$, where δ_ϵ is a regularized approximation of the delta distribution, sometimes referred to as blob approximations when studying vortex dynamics [6, 7]. This approach has also been applied in other fields, for example in plasma physics [19], where a piecewise approximation to the delta function was introduced. Although the blob approximations converge to the unregularized system as $\epsilon \rightarrow 0$, blobs with small ϵ generate large variations in $\frac{\partial G^\epsilon}{\partial r}$, leading to severe time-step restrictions when resolving the evolution dynamics. The quality of different delta distribution regularizations has recently been analyzed in a functional analysis setting [12]. Alternatively, one can

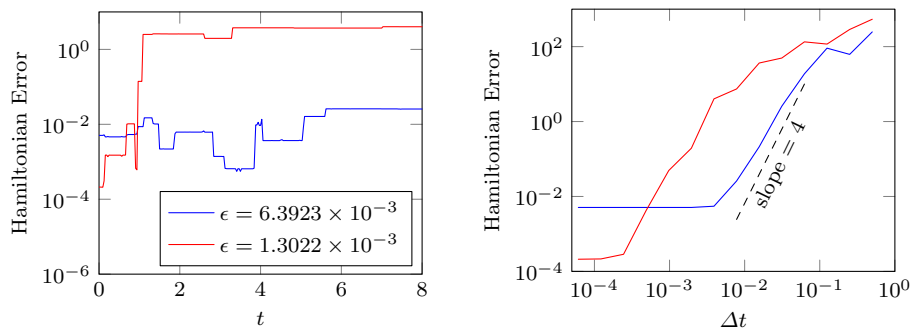


Fig. 2: *Left*: The Hamiltonian as a function of time when the regularized equation (2) is integrated with a fourth-order symplectic integrator with $\Delta t = 3.91 \times 10^{-3}$. Although a smaller ϵ results in a smaller modelling error initially (at $t = 0$), the steeper gradient in the kernel causes the time discretization error to dominate. *Right*: The error of the Hamiltonian at the time horizon $T = 8$ for various time step sizes. The dashed black line indicates fourth-order convergence.

replace the fundamental solution with a regularized version. For example, a regularized fundamental solution might satisfy $\Delta G^\epsilon(r) = n(\epsilon)\Delta G(r)s(r/\epsilon)$ [2], where $s(r)$ is a shape function satisfying

$$s(r) = \text{erf}(r) - \frac{2}{\sqrt{\pi}}re^{-r^2},$$

sometimes referred to as a Gaussian mollifier, and $n(\epsilon)$ is some normalizing factor that depends on the regularization ϵ . Different filters or mollifiers can also be used [11], but as before, small ϵ generate large variations in $\frac{\partial G^\epsilon}{\partial r}$. This paper replaces the fundamental solution with a two-parameter algebraic regularized kernel. Previously, one-parameter algebraic regularizations, equation (3), have been used in plasma physics [5, 10, 25], and for vortex sheet computations in fluid dynamics [16, 18, 24]. The modeling error that arises from the one-parameter family of regularized kernels is undesirable for practical values of ϵ .

1.3 Paper outline

This paper seeks new regularizations that reduce modelling error while allowing an integrator to realize these improved modelling error with large time steps. In Section 2, a two-parameter family of regularized kernels is introduced along with a notion of a global smoothing error, which will be used to quantify the quality of the regularized kernels and how they impact a numerical simulation. In Section 3, the Laplacian of the two-parameter family of regularized potentials is shown to converge to the delta function. In Section 4, the global smoothing errors of the two-parameter family of regularized kernels is analyzed. The regularized potentials are used to solve various N -body problems in Section 5. Finally, in Section 6, we summarize the results and discuss future work.

2 Regularized kernels

2.1 Two-parameter family of regularized kernels

A two-parameter family of algebraic regularized kernels can be constructed by taking the binomial or Taylor expansion of the non-regularized kernels,

$$G(r) = \begin{cases} -\frac{1}{2}(r^2 + \epsilon^2 - \epsilon^2)^{1/2} & \text{in } \mathbb{R}^1, \\ -\frac{1}{4\pi} \ln(r^2 + \epsilon^2) - \frac{1}{4\pi} \ln(1 - \epsilon^2(r^2 + \epsilon^2)^{-1}) & \text{in } \mathbb{R}^2, \\ \frac{1}{4\pi}(r^2 + \epsilon^2 - \epsilon^2)^{-1/2} & \text{in } \mathbb{R}^3, \end{cases}$$

and then truncating the expansion after n terms,

$$G^{\epsilon,n}(r) = \begin{cases} -\frac{1}{2} \sum_{\ell=0}^n \binom{\frac{1}{2}}{\ell} (-\epsilon^2)^\ell (r^2 + \epsilon^2)^{1/2-\ell} & \text{in } \mathbb{R}^1, \\ -\frac{1}{4\pi} \ln(r^2 + \epsilon^2) + \frac{1}{4\pi} \sum_{\ell=1}^n \frac{1}{\ell} \epsilon^{2\ell} (r^2 + \epsilon^2)^{-\ell} & \text{in } \mathbb{R}^2, \\ \frac{1}{4\pi} \sum_{\ell=0}^n \binom{-\frac{1}{2}}{\ell} (-\epsilon^2)^\ell (r^2 + \epsilon^2)^{-1/2-\ell} & \text{in } \mathbb{R}^3, \end{cases}$$

where ϵ is the perturbation size. The generalized binomial coefficient is defined as

$$\binom{\alpha}{\ell} = \frac{(\alpha)_\ell}{\ell!} = \frac{1}{\ell!} \prod_{k=0}^{\ell-1} (\alpha - k),$$

where $\alpha \in \mathbb{R}$ and $(\alpha)_\ell$ is the falling factorial. By construction, for any $\epsilon > 0$ and $r \neq 0$, $G^{\epsilon,n}(r) \rightarrow G(r)$ pointwise as $n \rightarrow \infty$. Note that when $n = 0$, the one-parameter family of regularized kernels, equation (3), is recovered.

2.2 Hamiltonian of a regularized system

If a time integrator is used to generate an approximate numerical solution to the system

$$\ddot{\mathbf{x}}_j = - \sum_{k \neq j} w_{jk} \nabla G^{\epsilon,n}(\mathbf{x}_j - \mathbf{x}_k), \quad (4)$$

the resulting error in the Hamiltonian can be decomposed into two parts: the modelling error that arises from replacing $\nabla_{\mathbf{x}} G(\|\mathbf{x} - \mathbf{y}\|)$ with $\nabla_{\mathbf{x}} G^{\epsilon,n}(\|\mathbf{x} - \mathbf{y}\|)$, and the time-stepping error associated with discrete time integration. The error in the Hamiltonian can be bounded,

$$|H^{\epsilon,n}(t) - H(0)| \leq |H^{\epsilon,n}(t) - H^{\epsilon,n}(0)| + |H^{\epsilon,n}(0) - H(0)|.$$

The first term is the time-stepping error, $|H^{\epsilon,n}(t) - H^{\epsilon,n}(0)|$, which depends on the chosen time step size. For $\epsilon > 0$ and $n \geq 0$, the time stepping error goes to zero as $\Delta t \rightarrow 0$. The rate at which this error term goes to zero depends, however,

on the size of the time step relative to $\nabla G^{\epsilon,n}$. The second term is the modelling or smoothing error, and satisfies

$$|H^{\epsilon,n}(0) - H(0)| = \left| \sum_j \sum_{k \neq j} w_{jk} (G^{\epsilon,n}(\mathbf{x}_j - \mathbf{x}_k) - G(\mathbf{x}_j - \mathbf{x}_k)) \right|. \quad (5)$$

In the numerical experiments in Section 5, the quantity $|H^{\epsilon,n}(T) - H(0)|$ will be reported for various choices of ϵ , n , and Δt .

2.3 Global smoothing errors

Since the regularized system, equation (4), relies on the gradient of the regularized kernels, we investigate the error of the gradient. One way to quantify the quality of the regularization is to measure the *global smoothing error*,

$$e[\epsilon, n] = \begin{cases} 2 \int_0^\infty \left| \frac{\partial G^{\epsilon,n}(r)}{\partial r} - \frac{\partial G(r)}{\partial r} \right| dr & \text{in } \mathbb{R}^1, \\ \int_0^\infty \left| \frac{\partial G^{\epsilon,n}(r)}{\partial r} - \frac{\partial G(r)}{\partial r} \right| 2\pi r dr & \text{in } \mathbb{R}^2, \\ \int_0^\infty \left| \frac{\partial G^{\epsilon,n}(r)}{\partial r} - \frac{\partial G(r)}{\partial r} \right| 4\pi r^2 dr & \text{in } \mathbb{R}^3, \end{cases} \quad (6)$$

where the gradient of the regularized kernels are

$$\frac{\partial G^{\epsilon,n}(r)}{\partial r} = \begin{cases} -r \sum_{\ell=0}^n \binom{\frac{1}{2}}{\ell} (-\epsilon^2)^\ell \left(\frac{1}{2} - \ell\right) (r^2 + \epsilon^2)^{-1/2-\ell} & \text{in } \mathbb{R}^1, \\ -\frac{r}{2\pi} \sum_{\ell=0}^n \epsilon^{2\ell} (r^2 + \epsilon^2)^{-\ell-1} & \text{in } \mathbb{R}^2, \\ -\frac{r}{2\pi} \sum_{\ell=0}^n \binom{-\frac{1}{2}}{\ell} (-\epsilon^2)^\ell \left(-\frac{1}{2} - \ell\right) (r^2 + \epsilon^2)^{-3/2-\ell} & \text{in } \mathbb{R}^3. \end{cases} \quad (7)$$

If $r = 0$, $\frac{\partial G^{\epsilon,n}(r)}{\partial r} = 0$ which is consistent with the physical argument that a particle does not feel any self-force. In \mathbb{R}^2 , the expression for $\frac{\partial}{\partial r} G^{\epsilon,n}(r)$ is a geometric series, leading to the simplified expression

$$\frac{\partial G^{\epsilon,n}(r)}{\partial r} = -\frac{1}{2\pi r} \left(1 - \left(\frac{\epsilon^2}{\epsilon^2 + r^2} \right)^{n+1} \right). \quad (8)$$

While this results in a more efficient expression for the gradient of the regularized kernel, similar simplifications in \mathbb{R}^1 and \mathbb{R}^3 do not exist. The difference between the gradient of the regularized and non-regularized kernels is

$$\frac{\partial}{\partial r} (G^{\epsilon,n}(r) - G(r)) = \begin{cases} \sum_{\ell=n+1}^{\infty} 2r \binom{\frac{1}{2}}{\ell} \binom{\frac{1}{2}}{\ell} (-1)^\ell \epsilon^{2\ell} (r^2 + \epsilon^2)^{-\frac{1}{2}-\ell} & \text{in } \mathbb{R}^1, \\ \frac{1}{2\pi r} \left(\frac{\epsilon^2}{\epsilon^2 + r^2} \right)^{n+1} & \text{in } \mathbb{R}^2, \\ \frac{r}{2\pi} \sum_{\ell=n+1}^{\infty} \binom{-\frac{1}{2}}{\ell} (-\epsilon^2)^\ell \left(-\frac{1}{2} - \ell\right) (r^2 + \epsilon^2)^{-3/2-\ell} & \text{in } \mathbb{R}^3, \end{cases}$$

n	$\epsilon (\mathbb{R}^1)$	$\epsilon (\mathbb{R}^2)$	$\epsilon (\mathbb{R}^3)$	Table 1: Values of ϵ and n that result in a global smoothing error of 10^{-2} . These pairings will be used in Figures 6, 8, 10, 13, and 15.
0	1.0051×10^{-2}	6.3923×10^{-3}	5.0189×10^{-3}	
1	2.0001×10^{-2}	1.2733×10^{-2}	1.0001×10^{-2}	
2	2.6667×10^{-2}	1.6977×10^{-2}	1.3333×10^{-2}	
4	3.6572×10^{-2}	2.3283×10^{-2}	1.8286×10^{-2}	
10	5.6755×10^{-2}	3.6132×10^{-2}	2.8378×10^{-2}	

where we have used equation (8) to eliminate the summation in \mathbb{R}^2 . The smoothing error, equation (6), is computed by integrating these expressions. In Section 4, we provide estimates and bounds for the global smoothing error.

We are interested in pairings (ϵ, n) that give rise to kernels with the same global smoothing error, equation (6). The global smoothing error can be approximated by truncating the infinite integral at 1, i.e.

$$\int_{B(0,1)} |\nabla G^{\epsilon,n} - \nabla G| d\mathbf{x} = 10^{-2}, \quad (9)$$

where $B(0, 1)$ is the unit ball centered at the origin in the appropriate dimension. This will facilitate a fair comparison (same global smoothing error) between lower-order (small n) and higher-order (large n) kernels. Figure 3 shows the pointwise error, equation (7), for various kernels that satisfy equation (9). For larger values of n , the error in the far field is greatly reduced without introducing sharp derivatives near the singularity.

The pairings (ϵ, n) used to generate the curves with fixed global smoothing error in Figure 3 are summarized in Table 1. Instead of computing the global smoothing error exactly, we satisfy equation (9) by applying the trapezoid rule on a sufficiently refined grid. By choosing these (ϵ, n) pairings, the numerical experiments in Section 5 will demonstrate that although the global smoothing error (i.e. a measure of the error in the gradient) is held fixed, the modelling error, equation (5), can be decreased with larger values of n .

3 Validity of the two-parameter family of regularized kernels

This section demonstrates that the two-parameter family of regularized kernels tend to the fundamental solutions for the Laplacian operator. Specifically, we will show that for any $\epsilon > 0$, $\Delta G^{\epsilon,n}(\mathbf{x}) \rightarrow \Delta G(\mathbf{x}) = -\delta(\mathbf{x})$ as $n \rightarrow \infty$, and that for any n , $\Delta G^{\epsilon,n}(\mathbf{x}) \rightarrow -\delta(\mathbf{x})$ as $\epsilon \rightarrow 0$, where δ is the delta function. All the convergences are understood to be taken in the weak sense. To check this convergence, we will show that $\Delta G^{\epsilon,n}(\mathbf{x}) \rightarrow 0$ for all $\mathbf{x} \neq 0$, and that $\int \Delta G^{\epsilon,n}(\mathbf{x}) d\mathbf{x}$ converges to -1 . This implies that $G^{\epsilon,n}(r)$ converges to the fundamental solution of the Laplacian operator.

Remark 1 In general, if $G^{\epsilon,n}(\mathbf{x})$ converges pointwise to $G(\mathbf{x})$ for all $\mathbf{x} \neq 0$, then $\Delta G^{\epsilon,n}$ converges weakly to the delta function. However, we will prove this result directly for our particular choice of $G^{\epsilon,n}$ as this will lead to closed-form solutions of $\Delta G^{\epsilon,n}$ which may be useful in future work.

We first generate simplified expressions for $\Delta G^{\epsilon,n}$, which will simplify the proofs that the two-parameter family of regularized kernels tend to the fundamental solutions of the Laplace operator.

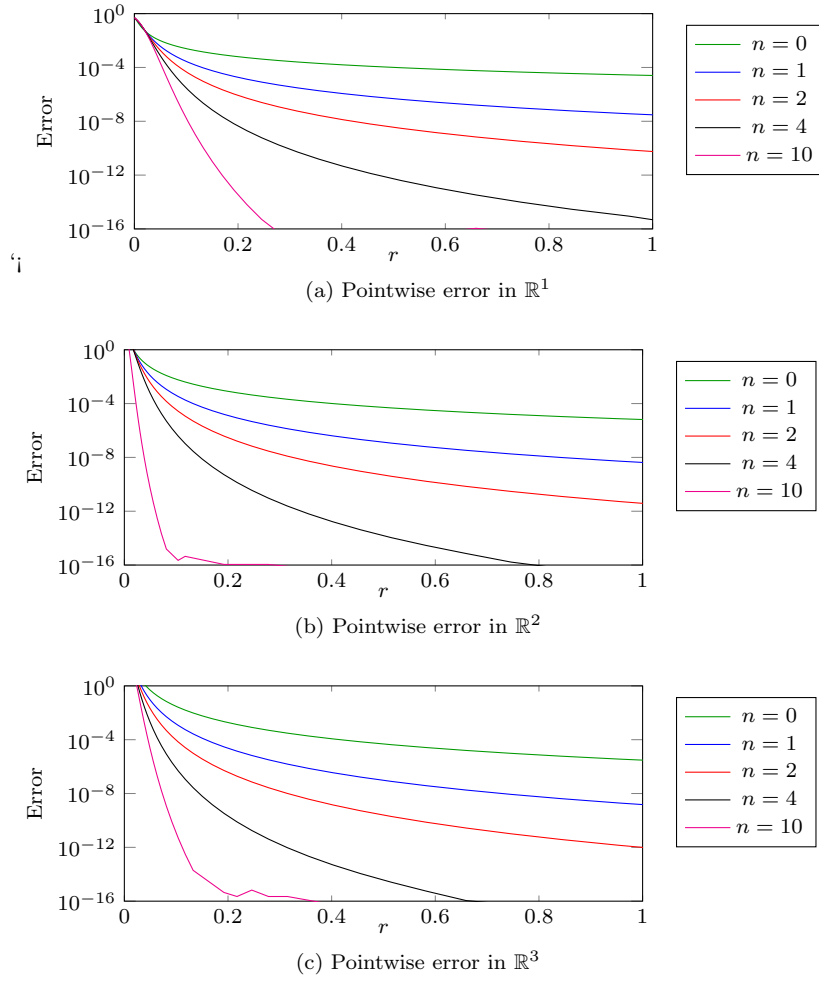


Fig. 3: Pointwise error of $\frac{\partial}{\partial r}(G^{\epsilon, n} - G)$ in \mathbb{R}^1 , \mathbb{R}^2 and \mathbb{R}^3 as a function of r for various (ϵ, n) pairings. The integral under each of these error curves is kept fixed.

3.1 Simplified expressions for $\Delta G^{\epsilon, n}(r)$

Applying the Laplacian operator to the two-parameter family of regularized kernels gives

$$\Delta G^{\epsilon, n}(r) = \begin{cases} -\sum_{\ell=0}^n \binom{\frac{1}{2}}{\ell} (-\epsilon^2)^\ell \left(\frac{1}{2} - \ell\right) (r^2 + \epsilon^2)^{-\frac{3}{2}-\ell} (-2\ell r^2 + \epsilon^2) & \text{in } \mathbb{R}^1, \\ -\frac{1}{\pi} \sum_{\ell=0}^n \epsilon^{2\ell} (r^2 + \epsilon^2)^{-\ell-2} (-\ell r^2 + \epsilon^2) & \text{in } \mathbb{R}^2, \\ -\frac{1}{2\pi} \sum_{\ell=0}^n \binom{-\frac{1}{2}}{\ell} (-\epsilon^2)^\ell \left(\frac{1}{2} + \ell\right) (r^2 + \epsilon^2)^{-\frac{5}{2}-\ell} (-2\ell r^2 + 3\epsilon^2) & \text{in } \mathbb{R}^3. \end{cases}$$

In \mathbb{R}^1 , the generalized binomial coefficients can be eliminated by using the identity

$$\binom{\frac{1}{2}}{\ell} \left(\frac{1}{2} - \ell\right) = \frac{(-1)^\ell \Gamma(\ell + \frac{1}{2})}{2\sqrt{\pi} \Gamma(\ell + 1)}.$$

Thus in \mathbb{R}^1 , the Laplacian operator applied to the two-parameter family of regularized kernels is

$$\begin{aligned} \Delta G^{\epsilon, n}(r) &= -\frac{1}{2\sqrt{\pi}} \sum_{\ell=0}^n \frac{\Gamma(\ell + \frac{1}{2})}{\Gamma(\ell + 1)} \epsilon^{2\ell} (r^2 + \epsilon^2)^{-\frac{3}{2}-\ell} (-2\ell r^2 + \epsilon^2) \\ &= -\frac{1}{2\epsilon\sqrt{\pi}} \sum_{\ell=0}^n \frac{\Gamma(\ell + \frac{1}{2})}{\Gamma(\ell + 1)} \frac{(-2\ell a^2 + 1)}{(a^2 + 1)^{\frac{3}{2}+\ell}} \end{aligned}$$

where $a = \frac{r}{\epsilon}$. Similarly, using the identity

$$\binom{-\frac{1}{2}}{\ell} \left(\frac{1}{2} + \ell\right) = \frac{(-1)^\ell \Gamma(\ell + \frac{3}{2})}{\sqrt{\pi} \Gamma(\ell + 1)},$$

the Laplacian of the two-parameter family of regularized kernels in \mathbb{R}^3 is

$$\Delta G^{\epsilon, n}(r) = -\frac{1}{2\pi\sqrt{\pi}\epsilon^3} \sum_{\ell=0}^n \frac{\Gamma(\ell + \frac{3}{2})}{\Gamma(\ell + 1)} \frac{(-2\ell a^2 + 3)}{(a^2 + 1)^{\frac{5}{2}+\ell}}.$$

These expressions for $\Delta G^{\epsilon, n}$ in \mathbb{R}^1 , \mathbb{R}^2 , and \mathbb{R}^3 can be simplified further so that there is no summation. These much simpler expressions allow us to verify that $\Delta G^{\epsilon, n}$ converges weakly to the delta function.

Theorem 1 *The Laplacian operator applied to the two-parameter family of regularized kernels can be expressed as*

$$\Delta G^{\epsilon, n}(r) = \begin{cases} -\frac{1}{\epsilon\sqrt{\pi}} \left(\frac{1}{1+a^2}\right)^{n+\frac{3}{2}} \frac{\Gamma(n+\frac{3}{2})}{\Gamma(n+1)} & \text{in } \mathbb{R}^1, \\ -\frac{(n+1)}{\pi\epsilon^2} \left(\frac{1}{1+a^2}\right)^{n+2} & \text{in } \mathbb{R}^2, \\ -\frac{1}{\epsilon^3\pi\sqrt{\pi}} \left(\frac{1}{1+a^2}\right)^{n+\frac{5}{2}} \frac{\Gamma(n+\frac{5}{2})}{\Gamma(n+1)} & \text{in } \mathbb{R}^3, \end{cases} \quad (10)$$

where $a = \frac{r}{\epsilon}$.

Proof In \mathbb{R}^1 , since $\Gamma(z+1) = z\Gamma(z)$, equation (10) holds for $n = 0$. Now, suppose equation (10) holds for $n = p$. Then,

$$\begin{aligned} \Delta G^{\epsilon, p+1}(r) &= -\frac{1}{\epsilon\sqrt{\pi}} \left(\frac{1}{1+a^2}\right)^{p+\frac{3}{2}} \frac{\Gamma(p+\frac{3}{2})}{\Gamma(p+1)} - \frac{\Gamma(p+\frac{3}{2})}{2\epsilon\sqrt{\pi}\Gamma(p+2)} \frac{(-2(p+1)a^2+1)}{(a^2+1)^{\frac{5}{2}+p}} \\ &= -\frac{1}{\epsilon\sqrt{\pi}} \left(\frac{1}{1+a^2}\right)^{p+\frac{5}{2}} \frac{\Gamma(p+\frac{3}{2})}{\Gamma(p+2)} \left[(1+a^2)\frac{\Gamma(p+2)}{\Gamma(p+1)} + \frac{(-2(p+1)a^2+1)}{2} \right] \\ &= -\frac{1}{\epsilon\sqrt{\pi}} \left(\frac{1}{1+a^2}\right)^{p+\frac{5}{2}} \frac{\Gamma(p+\frac{3}{2})}{\Gamma(p+2)} \left[(1+a^2)(p+1) + \frac{(-2(p+1)a^2+1)}{2} \right] \\ &= -\frac{1}{\epsilon\sqrt{\pi}} \left(\frac{1}{1+a^2}\right)^{p+\frac{5}{2}} \frac{\Gamma(p+\frac{3}{2})}{\Gamma(p+2)} \left(p+\frac{3}{2}\right) \\ &= -\frac{1}{\epsilon\sqrt{\pi}} \left(\frac{1}{1+a^2}\right)^{p+\frac{5}{2}} \frac{\Gamma(p+\frac{5}{2})}{\Gamma(p+2)}, \end{aligned}$$

which establishes that the equivalence must hold for $n = p+1$. A similar inductive argument can be used to establish equation (10) in \mathbb{R}^2 and \mathbb{R}^3 . \square

Remark 2 Since closed-form expressions (without the infinite summations) can be obtained for $\Delta G^{\epsilon, n}(r)$, one might expect that similar closed form expressions should exist for $\frac{\partial G^{\epsilon, n}(r)}{\partial r}$. This is unfortunately not the case in \mathbb{R}^1 and \mathbb{R}^3 , as previously noted.

3.2 Weak convergence to the delta function

Now that a closed-form expression for the Laplacian of the two-parameter family of regularized kernels has been attained, their weak limits can be shown to converge to the delta function.

Theorem 2 *The Laplacian of the two-parameter family of regularized kernels, $G^{\epsilon, n}(r)$, converges weakly to the delta function. That is,*

$$\lim_{n \rightarrow \infty} \Delta G^{\epsilon, n}(r) = -\delta(r) \text{ for any } \epsilon > 0, \quad (11)$$

$$\lim_{\epsilon \rightarrow 0} \Delta G^{\epsilon, n}(r) = -\delta(r) \text{ for any } n \geq 0. \quad (12)$$

Proof We first check that the two limits, equation (11) and equation (12) converge to 0 for all $r \neq 0$. If $\epsilon > 0$ and $r \neq 0$, then, from equation (10),

$$\lim_{n \rightarrow \infty} \Delta G^{\epsilon, n}(r) = 0,$$

for $\mathbb{R}^1, \mathbb{R}^2$ and \mathbb{R}^3 . Next, since equation (10) can be rewritten as

$$\Delta G^{\epsilon, n}(r) = \begin{cases} -\frac{\epsilon^{2n+2}}{\sqrt{\pi}} \left(\frac{1}{\epsilon^2+r^2}\right)^{n+\frac{3}{2}} \frac{\Gamma(n+\frac{3}{2})}{\Gamma(n+1)} & \text{in } \mathbb{R}^1, \\ -\frac{(n+1)\epsilon^{2n+2}}{\pi} \left(\frac{1}{\epsilon^2+r^2}\right)^{n+2} & \text{in } \mathbb{R}^2, \\ -\frac{\epsilon^{2n+2}}{\pi\sqrt{\pi}} \left(\frac{1}{\epsilon^2+r^2}\right)^{n+\frac{5}{2}} \frac{\Gamma(n+\frac{5}{2})}{\Gamma(n+1)} & \text{in } \mathbb{R}^3, \end{cases}$$

it follows that for any $n \geq 0$, $r \neq 0$,

$$\lim_{\epsilon \rightarrow 0} \Delta G^{\epsilon, n}(r) = 0.$$

Next, for all ϵ and n ,

$$\begin{aligned} 2 \int_0^\infty -\frac{1}{\epsilon\sqrt{\pi}} \left(\frac{1}{1 + \frac{r^2}{\epsilon^2}} \right)^{n+\frac{3}{2}} \frac{\Gamma(n + \frac{3}{2})}{\Gamma(n+1)} dr &= -1, \quad \text{in } \mathbb{R}^1, \\ -\frac{n+1}{\pi\epsilon^2} \int_0^\infty \left(\frac{1}{1 + \frac{r^2}{\epsilon^2}} \right)^{n+2} 2\pi r dr &= -1, \quad \text{in } \mathbb{R}^2, \\ -\frac{1}{\epsilon^3\pi\sqrt{\pi}} \int_0^\infty \left(\frac{1}{1 + \frac{r^2}{\epsilon^2}} \right)^{n+\frac{5}{2}} \frac{\Gamma(n + \frac{5}{2})}{\Gamma(n+1)} 4\pi r^2 dr &= -1, \quad \text{in } \mathbb{R}^3. \end{aligned}$$

Finally, let f be a compactly supported smooth function and $\epsilon > 0$. Then, for any $\alpha > 0$,

$$\int_{\mathbb{R}^d} \lim_{n \rightarrow \infty} \Delta G^{\epsilon, n}(\mathbf{x}) f(\mathbf{x}) d\mathbf{x} = \int_{B(0, \alpha)} \lim_{n \rightarrow \infty} \Delta G^{\epsilon, n}(\mathbf{x}) f(\mathbf{x}) d\mathbf{x}.$$

Since this holds for all $\alpha > 0$, we have

$$\begin{aligned} \int_{\mathbb{R}^d} \lim_{n \rightarrow \infty} \Delta G^{\epsilon, n}(\mathbf{x}) f(\mathbf{x}) d\mathbf{x} &= f(0) \int_{B(0, \alpha)} \lim_{n \rightarrow \infty} \Delta G^{\epsilon, n}(\mathbf{x}) d\mathbf{x} \\ &= f(0) \int_{\mathbb{R}^d} \lim_{n \rightarrow \infty} \Delta G^{\epsilon, n}(\mathbf{x}) d\mathbf{x} \\ &= -f(0), \end{aligned}$$

which establishes equation (11). The proof of equation (12) is similarly proved by fixing $n > 0$ and showing that

$$\int_{\mathbb{R}^d} \lim_{\epsilon \rightarrow 0} \Delta G^{\epsilon, n}(\mathbf{x}) f(\mathbf{x}) d\mathbf{x} = -f(0).$$

□

4 Error analysis

In this section we provide estimates of the global smoothing error, equation (6), that arises from using the two-parameter family of regularized kernels in \mathbb{R}^1 , \mathbb{R}^2 and \mathbb{R}^3 . In all three dimensions, we assume that the point masses are contained in the ball of radius R centered at the origin.

4.1 Global smoothing error in \mathbb{R}^1

We start by bounding

$$S[\epsilon, n] = 2 \sum_{\ell=n+1}^{\infty} \binom{\frac{1}{2}}{\ell} (-1)^\ell \left(z^{\ell-\frac{1}{2}} - 1 \right), \quad (13)$$

where $z = \frac{\epsilon^2}{R^2 + \epsilon^2} \in (0, 1)$, which will arise in our error estimate shortly.

Theorem 3 *Let S be defined in equation (13). For any $\epsilon > 0$,*

$$\lim_{n \rightarrow \infty} S[\epsilon, n] = 0.$$

Proof Since $z \in (0, 1)$, we can bound $S[\epsilon, 0]$ as

$$\begin{aligned} S[\epsilon, 0] &= 2 \sum_{\ell=1}^{\infty} \binom{\frac{1}{2}}{\ell} (-1)^\ell \left(z^{\ell-\frac{1}{2}} - 1 \right) \\ &= 2 \left(\frac{-\sqrt{z}}{1 + \sqrt{1-z}} + 1 \right) \in (0, 2). \end{aligned}$$

Therefore, since $S[\epsilon, 0]$ is bounded, this gives the desired result, that

$$\lim_{n \rightarrow \infty} S[\epsilon, n] = 0.$$

□

Next, the value of $S[\epsilon, n]$ is estimated. Define

$$g(z) := z^{-\frac{1}{2}} (S[\epsilon, 0] - 2) = \frac{-2}{1 + \sqrt{1-z}} = 2 \sum_{\ell=1}^{\infty} \binom{\frac{1}{2}}{\ell} (-1)^\ell z^{\ell-1}.$$

By Taylor's theorem, we have

$$2 \sum_{\ell=n+1}^{\infty} \binom{\frac{1}{2}}{\ell} (-1)^\ell z^{\ell-1} = \frac{-2}{1 + \sqrt{1-z}} - 2 \sum_{\ell=1}^n \binom{\frac{1}{2}}{\ell} (-1)^\ell z^{\ell-1} = \frac{g^{(n)}(\xi)}{n!} z^n, \quad (14)$$

where $\xi \in [0, z] \subset [0, 1)$. Multiplying both sides of equation (14) by $z^{\frac{1}{2}}$ gives,

$$2 \sum_{\ell=n+1}^{\infty} \binom{\frac{1}{2}}{\ell} (-1)^\ell z^{\ell-\frac{1}{2}} = \frac{g^{(n)}(\xi)}{n!} z^{n+\frac{1}{2}}. \quad (15)$$

Next, since

$$2 \sum_{\ell=1}^{\infty} \binom{\frac{1}{2}}{\ell} (-1)^\ell = -2,$$

this gives

$$2 \sum_{\ell=n+1}^{\infty} \binom{\frac{1}{2}}{\ell} (-1)^\ell = -2 - 2 \sum_{\ell=1}^n \binom{\frac{1}{2}}{\ell} (-1)^\ell. \quad (16)$$

Substituting equation (15) and equation (16) into equation (13) gives

$$S[\epsilon, n] = \left(\frac{g^{(n)}(\xi)}{n!} z^{n+\frac{1}{2}} + 2 \left(1 + \sum_{\ell=1}^n \binom{\frac{1}{2}}{\ell} (-1)^\ell \right) \right).$$

The global smoothing error (6) can be now be estimated as

$$\begin{aligned} e[\epsilon, n] &= 2 \int_0^R \left| \frac{\partial}{\partial r} (G^{\epsilon, n}(r) - G(r)) \right| dr \\ &= 2 \int_0^R \frac{\partial}{\partial r} \left(\sum_{\ell=n+1}^{\infty} \binom{\frac{1}{2}}{\ell} (-1)^\ell \epsilon^{2\ell} (r^2 + \epsilon^2)^{\frac{1}{2}-\ell} \right) dr \\ &= 2 \left(\sum_{\ell=n+1}^{\infty} \binom{\frac{1}{2}}{\ell} (-1)^\ell \epsilon^{2\ell} (r^2 + \epsilon^2)^{\frac{1}{2}-\ell} \right) \Big|_0^R \\ &= 2\epsilon \sum_{\ell=n+1}^{\infty} \binom{\frac{1}{2}}{\ell} (-1)^\ell \left(\left(\frac{\epsilon^2}{R^2 + \epsilon^2} \right)^{\ell-\frac{1}{2}} - 1 \right) \\ &= \epsilon S[\epsilon, n] \\ &= \epsilon \left(\frac{g^{(n)}(\xi)}{n!} \left(\frac{\epsilon^2}{R^2 + \epsilon^2} \right)^{n+\frac{1}{2}} + 2 \left(1 + \sum_{\ell=1}^n \binom{\frac{1}{2}}{\ell} (-1)^\ell \right) \right), \end{aligned}$$

where the absolute value was dropped since the derivative of each term in the summation is positive. This provides us with an estimate of the global smoothing error, and as expected, Theorem 3 guarantees that

$$\begin{aligned} \text{If } \epsilon > 0, \lim_{n \rightarrow \infty} e[\epsilon, n] &= 0, \\ \text{if } n \geq 0, \lim_{\epsilon \rightarrow 0} e[\epsilon, n] &= 0. \end{aligned}$$

4.2 Global smoothing error in \mathbb{R}^2

Following the analysis in \mathbb{R}^1 , we start by bounding

$$\begin{aligned} S[\epsilon, n] &= \sum_{\ell=n+1}^{\infty} \left(-\frac{1}{2\ell-1} \left(\frac{z}{1-z} \right)^{\ell-\frac{1}{2}} {}_2F_1 \left(\ell+1, \ell-\frac{1}{2}; \ell+\frac{1}{2}; -\frac{z}{1-z} \right) \right. \\ &\quad \left. - \frac{(-1)^\ell \pi^{\frac{3}{2}}}{4\ell! \Gamma(\frac{3}{2}-\ell)} \right), \end{aligned} \quad (17)$$

where $z = \frac{\epsilon^2}{R^2 + \epsilon^2} \in (0, 1)$, which will arise in the error estimate for \mathbb{R}^2 . The hypergeometric function is defined as

$${}_2F_1(a, b; c; z) = \sum_{n=0}^{\infty} \frac{(a)_n (b)_n}{(c)_n} \frac{z^n}{n!},$$

where $(a)_n = a(a-1)(a-2) \cdots (a-n+1)$ is the falling factorial, and $|z| < 1$.

Theorem 4 Let S be defined in equation (17). For any $\epsilon > 0$,

$$\lim_{n \rightarrow \infty} S[\epsilon, n] = 0.$$

Proof Unlike in \mathbb{R}^1 , we can not eliminate the summation in $S[\epsilon, n]$, but it can be partially simplified as

$$S[\epsilon, 0] = \frac{\pi}{2} - \sum_{\ell=1}^{\infty} \frac{1}{2^{\ell-1}} \left(\frac{z}{1-z} \right)^{\ell-\frac{1}{2}} {}_2F_1 \left(\ell+1, \ell-\frac{1}{2}; \ell+\frac{1}{2}, -\frac{z}{1-z} \right). \quad (18)$$

In Figure 4, we plot the 150 term partial sum of equation (18) which guarantees five digits of accuracy. Therefore, since $S[\epsilon, 0] \in (0, \frac{\pi}{2})$ is bounded, this gives the desired result, that

$$\lim_{n \rightarrow \infty} S[\epsilon, n] = 0.$$

□

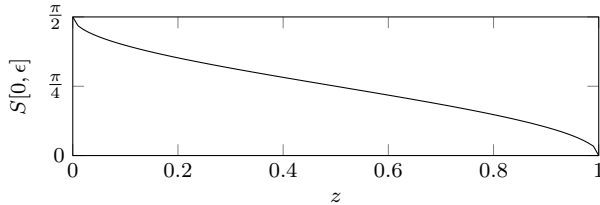


Fig. 4: A partial sum of equation (18). As desired, $S[\epsilon, 0]$ is bounded for $z \in (0, 1)$.

Without a closed-form expression for $S[\epsilon, n]$, we are unable to use Taylor's theorem to provide an estimate of $S[\epsilon, n]$. However, values of $S[\epsilon, n]$ can be computed by taking partial sums of equation (18). The global smoothing error, equation (6),

can be expressed in terms of $S[\epsilon, n]^1$,

$$\begin{aligned}
e[\epsilon, n] &= 2\pi \int_0^R r \left| \frac{\partial}{\partial r} (G^{\epsilon, n}(r) - G(r)) \right| dr \\
&= \int_0^R r^2 \left| \sum_{\ell=n+1}^{\infty} \epsilon^{2\ell} (r^2 + \epsilon^2)^{-\ell-1} \right| dr \\
&= \epsilon \sum_{\ell=n+1}^{\infty} \left\{ -\frac{1}{2\ell-1} \left(\frac{\epsilon}{R} \right)^{2\ell-1} {}_2F_1 \left(\ell+1, \ell - \frac{1}{2}; \ell + \frac{1}{2}, -\frac{\epsilon^2}{R^2} \right) \right. \\
&\quad \left. - \frac{(-1)^\ell \pi^{\frac{3}{2}}}{4\ell! \Gamma(\frac{3}{2} - \ell)} \right\} \\
&= \epsilon \sum_{\ell=n+1}^{\infty} \left\{ -\frac{1}{2\ell-1} \left(\frac{z}{1-z} \right)^{\ell-\frac{1}{2}} {}_2F_1 \left(\ell+1, \ell - \frac{1}{2}; \ell + \frac{1}{2}, -\frac{z}{1-z} \right) \right. \\
&\quad \left. - \frac{(-1)^\ell \pi^{\frac{3}{2}}}{4\ell! \Gamma(\frac{3}{2} - \ell)} \right\} \\
&= \epsilon S[\epsilon, n],
\end{aligned}$$

As expected, Theorem 4 guarantees that

$$\begin{aligned}
&\text{If } \epsilon > 0, \lim_{n \rightarrow \infty} e[\epsilon, n] = 0, \\
&\text{If } n \geq 0, \lim_{\epsilon \rightarrow 0} e[\epsilon, n] = 0.
\end{aligned}$$

4.3 Global smoothing error in \mathbb{R}^3

We start by bounding

$$\begin{aligned}
S[\epsilon, n] &= -\frac{2n+3}{2(n+1)} \binom{-\frac{1}{2}}{n} (-1)^n (z^{n+\frac{1}{2}} - 1) \\
&\quad - \frac{1}{2} \sum_{\ell=n+1}^{\infty} \binom{-\frac{1}{2}}{\ell} \frac{(-1)^\ell}{\ell+1} (z^{\ell+\frac{1}{2}} - 1), \tag{19}
\end{aligned}$$

where $z = \frac{\epsilon^2}{R^2 + \epsilon^2} \in (0, 1)$, which will arise in the error estimate.

Theorem 5 *Let S be defined in equation (19). For any $\epsilon > 0$,*

$$\lim_{n \rightarrow \infty} S[\epsilon, n] = 0.$$

¹ If the simplified expression for $\frac{\partial G^{\epsilon, n}}{\partial r}$ in equation (8) is used, one recovers the same expression involving the hypergeometric function.

Proof Since $z \in (0, 1)$, we can bound $S[\epsilon, 0]$ as

$$\begin{aligned} S[\epsilon, 0] &= -\frac{3}{2} \left(z^{\frac{1}{2}} - 1 \right) - \frac{1}{2} \sum_{\ell=1}^{\infty} \binom{-\frac{1}{2}}{\ell} \frac{(-1)^\ell}{\ell+1} \left(z^{\ell+\frac{1}{2}} - 1 \right) \\ &= 2 - \frac{3}{2} z^{\frac{1}{2}} - \frac{z^{\frac{3}{2}}}{2(1+\sqrt{1-z})^2} \in (0, 2). \end{aligned}$$

Therefore, since $S[\epsilon, 0]$ is bounded, this gives

$$\lim_{n \rightarrow \infty} S[\epsilon, n] = 0.$$

□

To estimate the value of $S[\epsilon, n]$, define

$$g(z) := -2z^{-\frac{3}{2}} \left(S[\epsilon, 0] - 2 + \frac{3}{2} z^{\frac{1}{2}} \right) = \frac{1}{(1+\sqrt{1-z})^2} = \sum_{\ell=1}^{\infty} \binom{-\frac{1}{2}}{\ell} \frac{(-1)^\ell}{\ell+1} z^{\ell-1}.$$

By Taylor's theorem, we have

$$\sum_{\ell=n+1}^{\infty} \binom{-\frac{1}{2}}{\ell} \frac{(-1)^\ell}{\ell+1} z^{\ell-1} = \frac{1}{(1+\sqrt{1-z})^2} - \sum_{\ell=1}^n \binom{-\frac{1}{2}}{\ell} \frac{(-1)^\ell}{\ell+1} z^{\ell-1} = \frac{g^{(n)}(\xi)}{n!} z^n,$$

where $\xi \in [0, z] \subset [0, 1)$. Multiplying both sides of the equation by $z^{\frac{3}{2}}$ gives,

$$\sum_{\ell=n+1}^{\infty} \binom{-\frac{1}{2}}{\ell} \frac{(-1)^\ell}{\ell+1} z^{\ell+\frac{1}{2}} = \frac{g^{(n)}(\xi)}{n!} z^{n+\frac{3}{2}}. \quad (20)$$

Next, since

$$\sum_{\ell=1}^{\infty} \binom{-\frac{1}{2}}{\ell} \frac{(-1)^\ell}{\ell+1} = 1,$$

we have

$$\sum_{\ell=n+1}^{\infty} \binom{-\frac{1}{2}}{\ell} \frac{(-1)^\ell}{\ell+1} = 1 - \sum_{\ell=1}^n \binom{-\frac{1}{2}}{\ell} \frac{(-1)^\ell}{\ell+1}. \quad (21)$$

Substituting equation (20) and equation (21) into equation (19), we have

$$\begin{aligned} S[\epsilon, n] &= -\frac{2n+3}{2(n+1)} \binom{-\frac{1}{2}}{n} (-1)^n \left(z^{n+\frac{1}{2}} - 1 \right) - \\ &\quad \frac{1}{2} \frac{g^{(n)}(\xi)}{n!} z^{n+\frac{3}{2}} + \frac{1}{2} \left(1 - \sum_{\ell=1}^n \binom{-\frac{1}{2}}{\ell} (-1)^\ell \frac{1}{\ell+1} \right). \end{aligned}$$

The global smoothing error can now be expressed in terms of $S[\epsilon, n]$,

$$\begin{aligned}
e[\epsilon, n] &= 4\pi \int_0^R r^2 \left| \frac{\partial}{\partial r} (G^{\epsilon, n}(r) - G(r)) \right| dr \\
&= 4\pi \int_0^R r^2 \left| \sum_{\ell=n+1}^{\infty} \frac{r}{2\pi} \binom{-\frac{1}{2}}{\ell} (-1)^\ell \epsilon^{2\ell} \left(-\frac{1}{2} - \ell\right) (r^2 + \epsilon^2)^{-\frac{3}{2} - \ell} \right| dr \\
&= 2 \sum_{\ell=n+1}^{\infty} \binom{-\frac{1}{2}}{\ell} (-1)^\ell \left(\frac{1}{2} + \ell\right) \epsilon^{2\ell} \int_0^R r^3 (r^2 + \epsilon^2)^{-\frac{3}{2} - \ell} dr \\
&= \sum_{\ell=n+1}^{\infty} \binom{-\frac{1}{2}}{\ell} (-1)^\ell \left(\frac{1}{2} + \ell\right) \epsilon^{2\ell} \int_{\epsilon^2}^{R^2 + \epsilon^2} (u - \epsilon^2) u^{-\frac{3}{2} - \ell} du \\
&= \epsilon \sum_{\ell=n+1}^{\infty} \binom{-\frac{1}{2}}{\ell} (-1)^\ell \left\{ \frac{\frac{1}{2} + \ell}{\frac{1}{2} - \ell} \left(\left(\frac{\epsilon^2}{R^2 + \epsilon^2} \right)^{\ell - \frac{1}{2}} - 1 \right) \right. \\
&\quad \left. + \left(\left(\frac{\epsilon^2}{R^2 + \epsilon^2} \right)^{\ell + \frac{1}{2}} - 1 \right) \right\},
\end{aligned}$$

where the absolute value can be dropped since each term in the summation is positive. By shifting indices and using standard properties of the generalized binomial coefficient, we have

$$\begin{aligned}
e[\epsilon, n] &= \epsilon \sum_{\ell=n+1}^{\infty} \binom{-\frac{1}{2}}{\ell} (-1)^\ell \left(\left(\frac{\epsilon^2}{R^2 + \epsilon^2} \right)^{\ell + \frac{1}{2}} - 1 \right) \\
&\quad - \epsilon \sum_{\ell=n}^{\infty} \frac{2\ell + 3}{2(\ell + 1)} \binom{-\frac{1}{2}}{\ell} (-1)^\ell \left(\left(\frac{\epsilon^2}{R^2 + \epsilon^2} \right)^{\ell + \frac{1}{2}} - 1 \right) \\
&= \epsilon \left\{ -\frac{2n + 3}{2(n + 1)} \binom{-\frac{1}{2}}{n} (-1)^n \left(\left(\frac{\epsilon^2}{R^2 + \epsilon^2} \right)^{n + \frac{1}{2}} - 1 \right) - \right. \\
&\quad \left. - \frac{1}{2} \sum_{\ell=n+1}^{\infty} \binom{-\frac{1}{2}}{\ell} (-1)^\ell \frac{1}{\ell + 1} \left(\left(\frac{\epsilon^2}{R^2 + \epsilon^2} \right)^{\ell + \frac{1}{2}} - 1 \right) \right\} \\
&= \epsilon S[\epsilon, n] \\
&= \epsilon \left\{ -\frac{2n + 3}{2(n + 1)} \binom{-\frac{1}{2}}{n} (-1)^n \left(\left(\frac{\epsilon^2}{R^2 + \epsilon^2} \right)^{n + \frac{1}{2}} - 1 \right) \right. \\
&\quad \left. - \frac{1}{2} \frac{g^{(n)}(\xi)}{n!} \left(\frac{\epsilon^2}{R^2 + \epsilon^2} \right)^{n + \frac{3}{2}} + \frac{1}{2} \left(1 - \sum_{\ell=1}^n \binom{-\frac{1}{2}}{\ell} (-1)^\ell \frac{1}{\ell + 1} \right) \right\}.
\end{aligned}$$

This provides us with an estimate of the global smoothing error. Invoking Theorem 5 guarantees that

$$\text{If } \epsilon > 0, \lim_{n \rightarrow \infty} e[\epsilon, n] = 0,$$

$$\text{If } n \geq 0, \lim_{\epsilon \rightarrow 0} e[\epsilon, n] = 0.$$

n	$\epsilon (\mathbb{R}^1)$	$\epsilon (\mathbb{R}^2)$	$\epsilon (\mathbb{R}^3)$
0	7.9753×10^{-4}	1.3022×10^{-3}	6.2537×10^{-4}
1	2.0001×10^{-2}	3.0382×10^{-2}	1.2038×10^{-2}
2	5.2761×10^{-2}	8.3471×10^{-2}	3.1985×10^{-2}
4	1.1366×10^{-1}	1.8888×10^{-1}	7.1597×10^{-2}
10	2.3711×10^{-1}	4.1171×10^{-1}	1.5639×10^{-1}

Table 2: Values of ϵ and n used in Figures 7, 11 and 14. With the presented initial conditions, each pairing gives a regularized kernel that results in the same modelling error, equation (5), of 4.89×10^{-6} .

5 Numerical Examples

We first demonstrate the described behaviors in $\mathbb{R}^1, \mathbb{R}^2$ and \mathbb{R}^3 for a dynamical system with two particles of equal mass—one with a positive unit charge and the other with a unit negative charge. Two different sets of (ϵ, n) pairings are used. Those in Table 1 keep the global smoothing error fixed at 10^{-2} , as described in equation (9). The pairings reported in Table 2 keep the modelling error, equation (5), fixed at 4.89×10^{-6} . Note that the modelling error depends on the initial condition whereas the global smoothing error does not. We conclude the numerical experiments by simulating 5 particles with an initial condition that results in a periodic orbit.

5.1 Harmonic oscillator in \mathbb{R}^1

The unregularized system is simply

$$\ddot{x}_j = \frac{1}{2} \sum_{k \neq j} \begin{cases} -1 & x_j > x_k, \\ 1 & x_j < x_k. \end{cases}$$

We consider two particles initially located at -0.125 and 0.125. To break the symmetry of the problem, which can cause errors to cancel, we set the initial velocity of the left particle to be 0.1 and the right particle to be 0. Applying a fourth-order symplectic integrator, we see in Figure 5 that whenever the particles cross, there is a jump in the error of the Hamiltonian. This jump is caused by the lack of regularity of the derivative of the Green's function. If there are only a few particles, it is possible to exactly fix the jump in the Hamiltonian by using an adaptive time step size. However, this strategy is not practical for many particles, or in higher dimensions. As an alternative, we replace the singular kernel with a regularized kernel. While the jumps are still present when using a regularized kernel because of large derivatives, they are much smaller than those for the unregularized system.

While the use of regularized kernels reduces the size of the jumps in the Hamiltonian error, it does introduce a modelling error. In Figure 6, we plot the error in the Hamiltonian for six different regularizations: the unregularized kernel, and kernels regularized with the (ϵ, n) pairings in Table 1. These pairings are specifically chosen because each (ϵ, n) pair has the same global regularization error. For large Δt , there is no benefit in using the high-order regularized kernels. However,

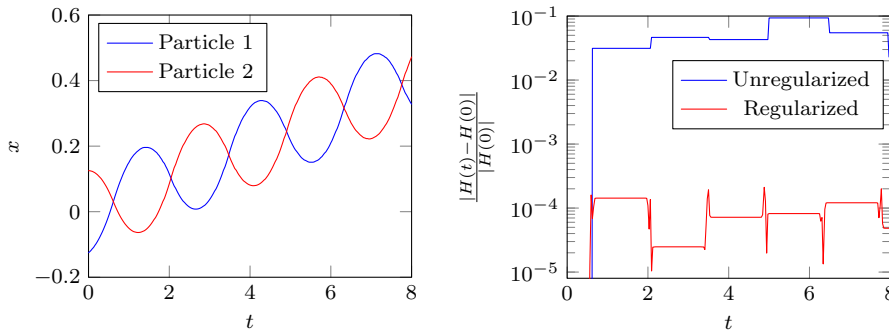


Fig. 5: The positions of the particles (left) and the errors in the Hamiltonian (right) when using the unregularized potential and regularized potential in \mathbb{R}^1 . Time stepping was done with a fourth-order symplectic integrator. In this example, the time step size is 3.125×10^{-2} and the smoothing regularization parameter pairing is $(\epsilon, n) = (5.6755 \times 10^{-2}, 10)$.

if smaller errors need to be achieved, then it is favorable to use a regularized kernel. Furthermore, we see that our new regularized kernels, $n > 0$, achieve smaller modelling errors, even though they have the same global smoothing error defined in equation (6).

It could be argued that the regularization error can be simply decreased by taking a smaller value for ϵ while keeping n fixed. However, if ϵ is decreased, the derivative of the regularized kernel increases at the origin, and the result is a smaller asymptotic region for fourth-order convergence. In Figure 7, we compare the error in the Hamiltonian for (ϵ, n) pairings that all have a modelling error of 4.89×10^{-6} . Using larger values of n results in larger regions of fourth-order convergence. The trade-off is the increased computational complexity for evaluating higher-order kernels.

Finally, we examine the phase plane of the variable $z(t) = x_1(t) - x_2(t)$. We increase the time horizon from $T = 8$ to $T = 400$ and keep the time step size fixed at 3.125×10^{-2} . In Figure 8, we plot the position $z(t)$ versus the velocity $\dot{z}(t)$ resulting from the unregularized potential and the regularized potential with $n = 10, \epsilon = 5.6755 \times 10^{-2}$; the phase portrait with the other (ϵ, n) pairings in Table 1 are indistinguishable in the eyeball norm from the $n = 10$ kernel. The phase portrait of the unregularized system shows the effect of the truncation error due to a discrete time integrator being used in conjunction with the singular kernel. The qualitative periodic nature of the oscillations are perturbed. On the other hand, the regularized kernels significantly reduce the truncation error, better preserving the periodic nature of the orbits. If one were to compare the final solutions using the regularized kernels using the (ϵ, n) pairings in Table 1, the errors would decrease with increasing n (not shown).

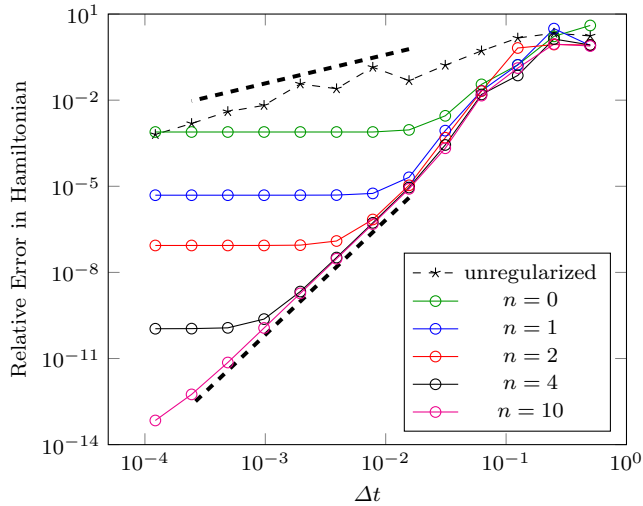


Fig. 6: The error in the Hamiltonian arising from using kernel regularization in \mathbb{R}^1 with pairings of (ϵ, n) in Table 1. While fourth-order convergence is eventually achieved for all (ϵ, n) pairs, the error eventually plateaus due to the modelling error of solving a regularized system. Although the (ϵ, n) pairs have the same global regularization error, smaller modelling errors can be achieved when the higher-order kernels are used. The dashed black lines correspond to first- and fourth-order convergence.

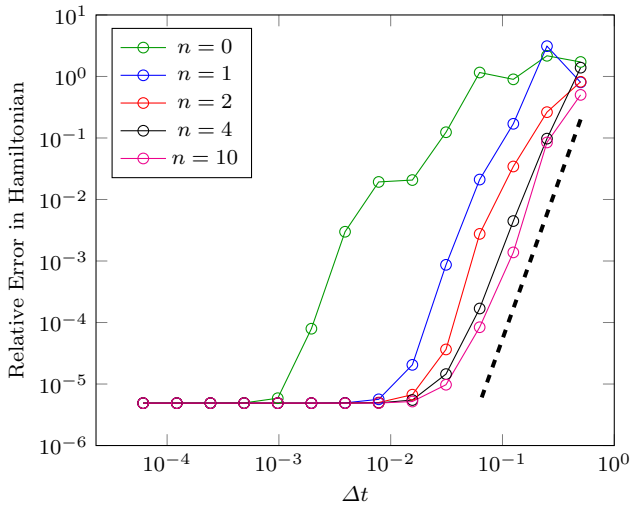


Fig. 7: The error in the Hamiltonian arising from using kernel regularization in \mathbb{R}^1 with pairings of (ϵ, n) in Table 2. Higher-order kernels have smoother transition regions, allowing for high-order convergence with larger time step sizes. The dashed black line corresponds to fourth-order convergence.

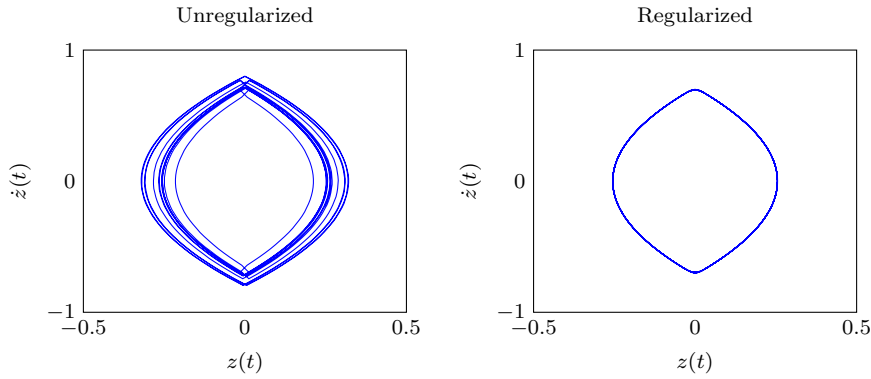


Fig. 8: The phase field of the $z(t) = x_1(t) - x_2(t)$. The regularized potentials maintain the periodic solution of the problem for coarse time steps.

5.2 Harmonic oscillator in \mathbb{R}^2

Two particles are initially placed at $(-0.25, 0)$ and $(0.25, 0)$ with initial velocities $(0, 10^{-3})$ and $(0, 0)$ respectively. The unregularized system is

$$\ddot{\mathbf{x}}_j = \frac{1}{2\pi} \sum_{k \neq j} \frac{\mathbf{x}_j - \mathbf{x}_k}{|\mathbf{x}_j - \mathbf{x}_k|^2}.$$

These initial conditions were chosen so that the particles come close to each other without actually passing through each other. We expect the close proximity of the particles to each other to delay the fourth-order convergence if the unregularized system is solved. In Figure 9, the distance between the two particles and the error in the Hamiltonian as a function of time is plotted. When the particles are close to each other, there is a jump in the error of the Hamiltonian.

Repeating the numerical experiments from Section 5.1, Figure 10 shows the convergence behavior of the regularized dynamical system if the (ϵ, n) pairings from Table 1 (fixed global smoothing error) are used. Similar observations to the experiment in \mathbb{R}^1 can be observed: the symplectic integrator achieves fourth-order accuracy for each regularized system for large Δt , until the modeling error dominates. If the (ϵ, n) pairings from Table 2 (fixed modelling error) are used, the higher-order regularized kernels exhibit fourth-order convergence for larger Δt (c.f. Figure 11).

5.3 Harmonic oscillator in \mathbb{R}^3

Similarly, we place 2 particles at $(-0.1, 0, 0)$ and $(0.1, 0, 0)$ with initial velocities of $(0, 10^{-3}, 0)$ and $\mathbf{0}$ respectively. The unregularized system is

$$\ddot{\mathbf{x}}_j = \frac{1}{4\pi} \sum_{k \neq j} \frac{\mathbf{x}_j - \mathbf{x}_k}{|\mathbf{x}_j - \mathbf{x}_k|^3}.$$

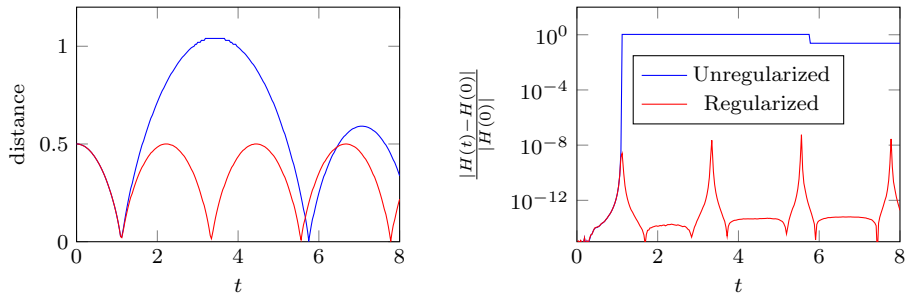


Fig. 9: The distance between the particles (left) and the errors in the Hamiltonian (right) when using the unregularized potential and regularized potential in \mathbb{R}^2 . Time stepping was done with a fourth-order symplectic integrator. In this example, the time step size is 4.88×10^{-4} and the smoothing regularization parameter pairing is $(\epsilon, n) = (3.6132 \times 10^{-2}, 10)$.

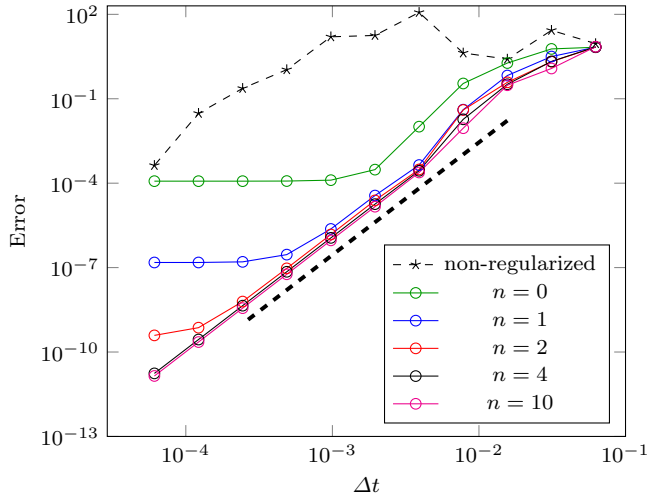


Fig. 10: The error in the Hamiltonian arising from using (ϵ, n) pairings in Table 1 for the oscillator in \mathbb{R}^2 . Fourth-order convergence is achieved for both the unregularized kernel and the regularized kernels. However, for the unregularized kernel, smaller time steps are required to enter this asymptotic regime. For the regularized systems, the error eventually plateaus when the modelling error dominates. By using larger values of n , smaller modelling errors can be achieved. The dashed black line corresponds to fourth-order convergence.

As before, we expect that the singularity will reduce the order of accuracy of the fourth-order symplectic integrator. In fact, since the singularity is even stronger than in \mathbb{R}^2 , we see that the unregularized system does not even obtain convergence for the reported values of Δt (Figure 13). By introducing a regularization, fourth-order convergence is observed. Again, as before, we observe that if the global smoothing error is kept constant, than larger values of n reduce the modelling

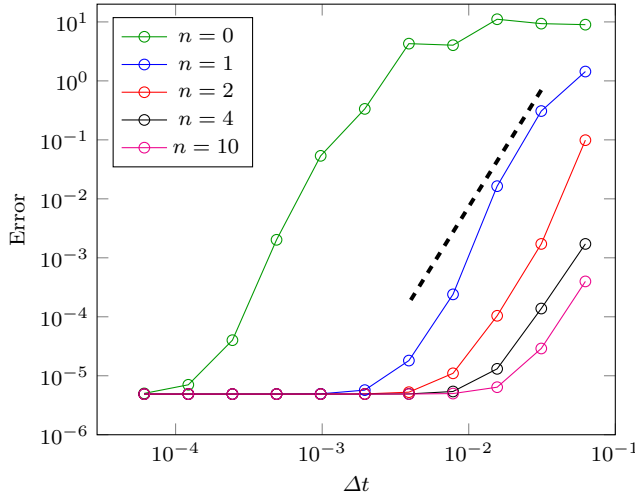


Fig. 11: The error in the Hamiltonian arising from using kernel regularization in \mathbb{R}^2 with pairings of (ϵ, n) that have the same modelling error (as opposed to the smoothing error) of 4.89×10^{-6} . Larger values of n achieve desired accuracies with larger time step sizes. The dashed black line corresponds to fourth-order convergence.

error, and we are able to achieve more accurate results. As in \mathbb{R}^1 , the benefit of using large values of n is illustrated in Figure 14. The modelling error is fixed at 4.89×10^{-6} , and the error in the Hamiltonian is plotted for the different (ϵ, n) pairings.

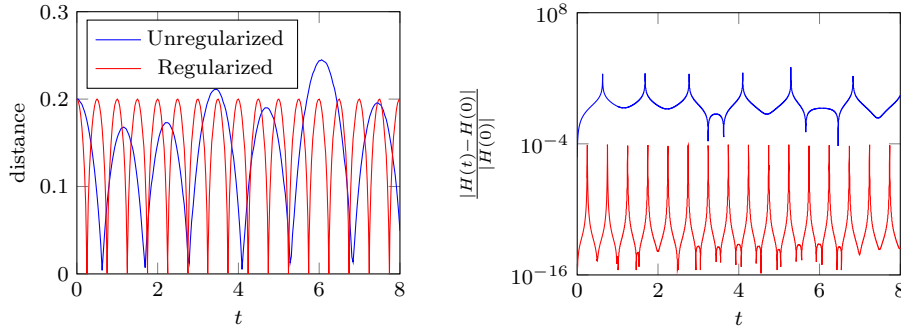


Fig. 12: The distance between the particles (left) and the errors in the Hamiltonian (right) when using the unregularized potential and regularized potential in \mathbb{R}^3 . Time stepping was done with a fourth-order symplectic integrator. In this example, the time step size is 2.44×10^{-4} and the smoothing regularization parameter pairing is $(\epsilon, n) = (2.8378 \times 10^{-2}, 10)$.

5.4 Periodic orbit in \mathbb{R}^3

We consider five particles in the $z = 0$ plane of \mathbb{R}^3 . We change the sign of $G(r)$ so that the Hamiltonian system corresponds to motion due to the gravitational potential. By setting the mass of each particle to $\sqrt{0.2}$, so that $w_{jk} = 2$, and using

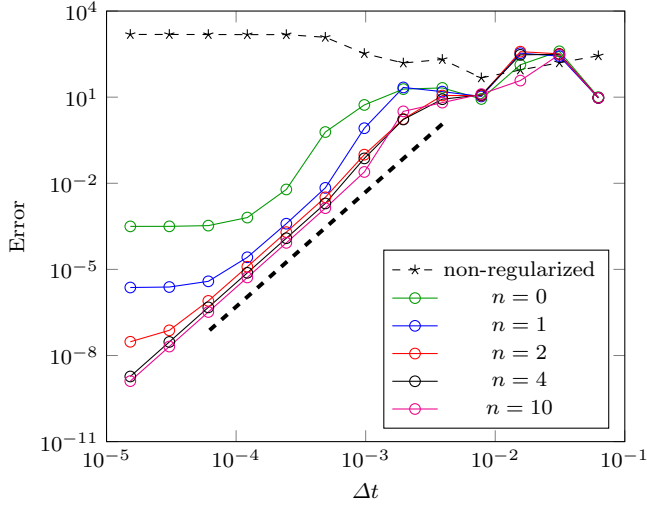


Fig. 13: The error in the Hamiltonian arising from using kernel regularization in \mathbb{R}^3 . While fourth-order convergence is achieved for all values of n , the error eventually plateaus. By using larger values of n , smaller errors can be achieved. The dashed black line corresponds to fourth-order convergence.

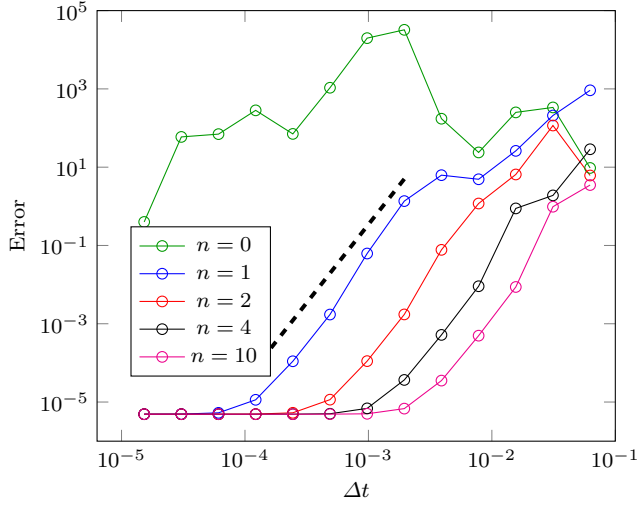


Fig. 14: The error in the Hamiltonian arising from using kernel regularization in \mathbb{R}^3 with pairings of (ϵ, n) that have the same regularization error of 4.89×10^{-6} . Larger values of n achieve desired accuracies with larger time step sizes. The dashed black line corresponds to fourth-order convergence.

the initial condition

$$\mathbf{x}(0) = \begin{pmatrix} +3.315332 \times 10^{-1} & 0 \\ +8.795500 \times 10^{-2} & -3.394340 \times 10^{-2} \\ -2.537216 \times 10^{-1} & -5.353020 \times 10^{-2} \\ -2.537216 \times 10^{-1} & +5.353020 \times 10^{-2} \\ +8.795500 \times 10^{-2} & +3.394340 \times 10^{-2} \end{pmatrix},$$

$$\dot{\mathbf{x}}(0) = \begin{pmatrix} 0 & -5.937860 \times 10^{-1} \\ +1.822785 \times 10^0 & +1.282480 \times 10^{-1} \\ +1.271564 \times 10^0 & +1.686450 \times 10^{-1} \\ -1.271564 \times 10^0 & +1.686450 \times 10^{-1} \\ -1.822785 \times 10^0 & +1.282480 \times 10^{-1} \end{pmatrix},$$

the dynamics should result in a periodic orbit with period $T = 2\pi/5$ [23]. Using a fourth-order symplectic integrator with 10^6 time steps, the non-regularized system does not give a periodic orbit, due to the singularity of the kernel. Using the (ϵ, n) pairings from Table 1 (i.e., fixed global smoothing error), the orbits of the regularized system are shown in Figure 15. For the $n = 0, 1, 2$ kernels, the modelling error dominates in the regularized system, resulting in orbits that are qualitatively different from the expected periodic orbit. The $n = 4$ and $n = 10$ kernels result in regularized systems that give qualitatively correct periodic orbits.

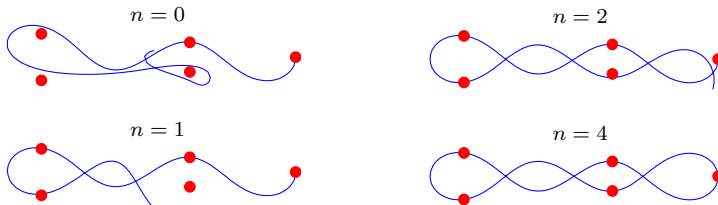


Fig. 15: The initial location of the five particles and the trajectory that one of the particles follows over one period. If n is too small, the correct orbit can not be achieved. However, with $n = 4$, the error in periodicity is 10^{-2} . The orbit with $n = 10$ looks similar to the orbit with $n = 4$.

The largest possible time step that keeps the relative error in periodicity bounded at 10^{-2} , i.e. $\|\mathbf{x}(T) - \mathbf{x}(0)\| < 10^{-2}\|\mathbf{x}(0)\|$, is computed for the $n = 4$ and $n = 10$ systems. The results are reported in Table 3. A larger time step can be used for the $n = 10$ kernels.

n	Δt	Period Error	Hamiltonian Error	Modelling Error
4	1.58×10^{-3}	9.99×10^{-3}	3.65×10^{-7}	2.50×10^{-7}
10	2.29×10^{-3}	9.98×10^{-3}	5.13×10^{-7}	9.87×10^{-11}

Table 3: A summary of the different errors when considering five particles that form a periodic orbit. We see that using $n = 10$ allows for a larger time step size than $n = 4$.

6 Conclusions

In this paper, we derived a new family of regularized kernels, suitable for simulating a Hamiltonian system that contains the fundamental solution of Laplace's equation using high-order time integrators. These high-order kernels were obtained by a Taylor expansion of the non-regularized kernel about $(r^2 + \epsilon^2)$ in \mathbb{R}^1 , \mathbb{R}^2 , and \mathbb{R}^3 . The analysis shows that the regularized kernels, $G^{\epsilon, n}(r)$, converge to the fundamental solution of Laplace's equation as $n \rightarrow \infty$ for any $\epsilon > 0$, and as $\epsilon \rightarrow 0$ for any $n \geq 0$. In addition to the derivation and validation of the high-order kernels, error bounds for the regularized solution were derived.

We have shown that these regularizations can reduce the error in the far field without introducing sharp derivatives near the singularity. This is particularly useful when applying high-order time stepping methods to a Hamiltonian system such as a harmonic oscillator. In particular, high-order regularized kernels (with identical global smoothing error) can reduce the modelling error of the regularized system. Alternatively, if one chooses regularizations that give rise to similar modelling errors, high-order accuracy can be achieved for larger time step sizes using these high-order kernels.

Future work includes using these high-order kernels within treecode algorithms for approximating the electric field arising from a charged particle system [3, 4, 22]—this is necessary when simulating a large number of particles. In a treecode computation, a Taylor series expansion of the regularized potential is needed for the computation of the cluster-particle interaction. While explicit formulas for the Taylor coefficients of the high-order regularized kernels can be derived and evaluated, the computational complexity might be prohibitive. The authors anticipate that a recurrence relation to evaluate the Taylor coefficients of the high-order regularized kernels can be recovered. Certainly, the recurrence relation for the $n = 0$ kernels are available [18]. Alternatively, a kernel-independent fast multipole method [20] can be used to significantly reduce the number of computations. With these fast algorithms, more complicated simulations such as vortex motions [14, 15] can be investigated. High-order regularized kernels can likely also be formulated in a similar fashion for for the screened Coulomb potential [17] or Winckelmans–Leonard kernel [24].

Acknowledgments

The authors would like to thank Robert Krasny, Keith Cartwright, John Verboncoeur, John Luginsland, Matthew Bettencourt, and Andrew Greenwood for their insightful discussions regarding this work, as well as anonymous referees who have made valuable suggestions to improve the presentation of this manuscript.

References

1. Bate, R.R., Mueller, D.D., White, J.E.: *Fundamentals of astrodynamics*. Courier Corporation (1971)
2. Beale, J.: A grid-based boundary integral method for elliptic problems in three dimensions. *SIAM Journal on Numerical Analysis* **42**(2), 599–620 (2004)
3. Christlieb, A., Krasny, R., Verboncoeur, J.: A treecode algorithm for simulating electron dynamics in a Penning–Malmberg trap. *Computer Physics Communications* **164**(1-3), 306–310 (2004)
4. Christlieb, A., Krasny, R., Verboncoeur, J.: Efficient particle simulation of a virtual cathode using a grid-free treecode Poisson solver. *Plasma Science, IEEE Transactions on* **32**(2 Part 1), 384–389 (2004)
5. Christlieb, A., Krasny, R., Verboncoeur, J., Emhoff, J., Boyd, I.: Grid-free plasma simulation techniques. *Plasma Science, IEEE Transactions on* **34**(2 Part 1), 149–165 (2006)
6. Cortez, R.: The Method of Regularized Stokeslets. *SIAM Journal on Scientific Computing* **23**(4), 1204–1225 (2001)
7. Cortez, R., Minion, M.: The blob projection method for immersed boundary problems. *Journal of Computational Physics* **161**(2), 428 – 453 (2000). DOI <http://dx.doi.org/10.1006/jcph.2000.6502>. URL <http://www.sciencedirect.com/science/article/pii/S0021999100965021>

8. Faou Erwanand Hairer, E., Pham, T.L.: Energy conservation with non-symplectic methods: Examples and counter-examples. *BIT Numerical Mathematics* **44**(4), 699–709 (2004). DOI 10.1007/s10543-004-5240-6. URL <http://dx.doi.org/10.1007/s10543-004-5240-6>
9. Forest, E., Ruth, R.D.: Fourth-order symplectic integration. *Phys. D* **43**(1), 105–117 (1990). DOI 10.1016/0167-2789(90)90019-L. URL [http://dx.doi.org/10.1016/0167-2789\(90\)90019-L](http://dx.doi.org/10.1016/0167-2789(90)90019-L)
10. Gibbon, P., Speck, R., Karmakar, A., Arnold, L., Frings, W., Berberich, B., Reiter, D., Masek, M.: Progress in Mesh-Free Plasma Simulation With Parallel Tree Codes. *Plasma Science, IEEE Transactions on* **38**(9), 2367–2376 (2010)
11. Hejlesen, M.M., Rasmussen, J.T., Chatelain, P., Walther, J.H.: A high order solver for the unbounded Poisson equation. *J. Comput. Phys.* **252**, 458–467 (2013). DOI 10.1016/j.jcp.2013.05.050. URL <http://dx.doi.org/10.1016/j.jcp.2013.05.050>
12. Hosseini, B., Nigam, N., Stockie, J.M.: On regularizations of the Dirac delta distribution. *J. Comput. Phys.* **305**, 423–447 (2016)
13. Jackson, J.D.: *Classical electrodynamics*. Wiley (1999)
14. Krasny, R.: Desingularization of periodic vortex sheet roll-up. *Journal of Computational Physics* **65**(2), 292–313 (1986)
15. Krasny, R.: Computation of vortex sheet roll-up in the Trefftz plane. *Journal of Fluid Mechanics* **184**, 123–155 (1987)
16. Leonard, A.: Vortex methods for flow simulation. *J. Comput. Phys.* **37**(3), 289–335 (1980). DOI 10.1016/0021-9991(80)90040-6. URL [http://dx.doi.org/10.1016/0021-9991\(80\)90040-6](http://dx.doi.org/10.1016/0021-9991(80)90040-6)
17. Li, P., Johnston, H., Krasny, R.: A cartesian treecode for screened coulomb interactions. *Journal of Computational Physics* **228**(10), 3858 – 3868 (2009). DOI <http://dx.doi.org/10.1016/j.jcp.2009.02.022>. URL <http://www.sciencedirect.com/science/article/pii/S0021999109000916>
18. Lindsay, K., Krasny, R.: A particle method and adaptive treecode for vortex sheet motion in three-dimensional flow. *Journal of Computational Physics* **172**(2), 879–907 (2001)
19. Majda, A., Majda, G., Zheng, Y.: Concentrations in the one-dimensional Vlasov-Poisson equations, I: Temporal development and non-unique weak solutions in the single component case. *Physica D* **74**(3-4), 268–300 (1994)
20. Rostami, M.W., Olson, S.D.: Kernel-Independent Fast Multipole Method within the framework of Regularized Stokeslets. *Journal of Fluids and Structures* (2015). Under review
21. Ruth, R.D.: A canonical integration technique. *IEEE Transactions on Nuclear Science* **30**(4), 2669–2671 (1983). DOI 10.1109/TNS.1983.4332919
22. Salmon, J., Warren, M.: Skeletons from the treecode closet. *Journal of Computational Physics* **111**(1), 136–155 (1994)
23. Simó, C.: New families of solutions in N-body problems. In: *European Congress of Mathematics*, pp. 101–115. Springer (2001)
24. Wee, D., Marzouk, Y.M., Schlegel, F., Ghoniem, A.F.: Convergence characteristics and computational cost of two algebraic kernels in vortex methods with a tree-code algorithm. *SIAM J. Sci. Comput.* **31**(4), 2510–2527 (2009). DOI 10.1137/080726872. URL <http://dx.doi.org/10.1137/080726872>
25. Winckelmans, G.S., Leonard, A.: Contributions to vortex particle methods for the computation of three-dimensional incompressible unsteady flows. *J. Comput. Phys.* **109**(2), 247–273 (1993). DOI 10.1006/jcph.1993.1216. URL <http://dx.doi.org/10.1006/jcph.1993.1216>